Bifurcation of the Pacific North Equatorial Current in a wind-driven model: response to climatological winds

Tommy G. Jensen

Abstract The sensitivity of the bifurcation of the North Equatorial Current in the Pacific to different wind products is investigated. Variations of the bifurcation latitude with season is simulated in a purely wind-driven model and is found to be in agreement with recent observations. The seasonal cycle is nearly independent of the wind climatology, but the annual average latitude depends on the wind stress curl. It is also shown that in the upper ocean, the poleward shift in bifurcation latitude with depth is realistic in our simple model. This implies that given a stratification close to the observed, it is primarily the wind forcing that determines the location of the bifurcation and its seasonal variation.

Keywords North Equatorial Current · Bifurcation · North Pacific · Numerical modeling

1 Introduction

The Pacific North Equatorial Current (NEC) bifurcates into the northward-flowing Kuroshio and southward-flowing Mindanao Current at the Philippine coast. An important role of these two western boundary currents is closing the mass budgets of the subtropical and

T. G. Jensen (✉)
Oceanography Division, Naval Research Laboratory,
Code 7322, Stennis Space Center, MS 39529-5004, USA
e-mail: Tommy.Jensen@nrlssc.navy.mil

tropical gyres, respectively, and the NEC bifurcation marks the separation of the two gyres at the western boundary. It is therefore of interest to understand the processes that control the location of the latitude.

1.1 Observations

The bifurcation latitude varies seasonally and with depth. Toole et al. (1990) noted a bifurcation latitude of 14.1° in September 1987, while it was observed to be at 12.6° in April 1988, suggesting a seasonal change, and Nitani (1972) first reported a poleward shift in bifurcation latitude with depth. Based on geostrophic calculations relative to 1,500 dbar from the Levitus (1982) annual mean climatology, Qu et al. (1998) showed that the NEC volume transport of 41 Sv bifurcates into a northward transport of 14 Sv and southward transport of 27 Sv; they also confirmed a northward shift in bifurcation latitude with depth from about 13.5° N at the surface to 18° N at 500 dbar in good agreement with the water property distributions (Qu et al. 1999).

In a recent comprehensive reanalysis of historical hydrography data, Qu and Lukas (2003) determined that the bifurcation for currents averaged over the upper 1,000 m occurs at 17.2° N in December and at 14.8° N in July. Its annual mean location was at 15.2° N, close to the estimate from Sverdrup theory (14.6° N), varying from 13.3° N near the surface to about 20° N at 1,000 m.

Qu and Lukas (2003) found the bifurcation latitude to be closest to the equator in June–July and at its northernmost position in December (Fig. 1). Throughout the year, the bifurcation latitude increases with depth, in particular during the boreal winter. Note that the bifurcation from observations is well-defined only

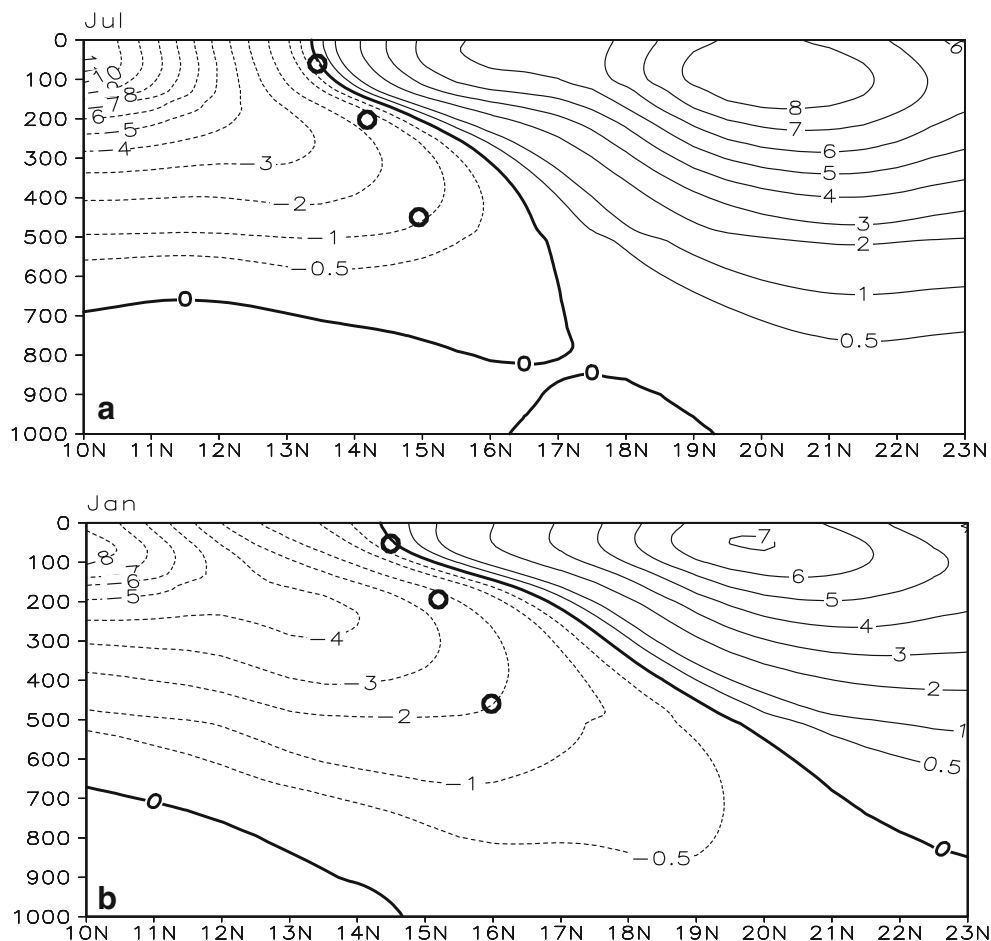**Fig. 1** Meridional current
component along the coast of
the Philippines in July (*top*)
and January (*bottom*). Unit is
centimeters per second. The
bifurcation latitudes from the
layer model forced by
ECMWF winds are shown by
filled circles (adapted from
Qu and Lukas 2003)

at depths less than about 500 m during the summer and
to about 600 m during the winter.

The motivation for this study is the above-mentioned
analysis by Qu and Lukas (2003), who determined the
annual cycle of the bifurcation based on hydrographic
observations. Their results are further confirmed by
recent results from a high-resolution ocean general
circulation model (OGCM) by Kim et al. (2004), but
differed significantly from earlier modeling results by
Qiu and Lukas (1996), who used a simple wind-driven
reduced gravity model and suggested that the bifurca-
tion was determined by the wind stress curl alone. The
discrepancy between the work of Qiu and Lukas (1996)
and the later research questions to what extent a sim-
ple wind-driven model is able to capture the essential
dynamics needed to reproduce a realistic bifurcation or
if additional vertical modes plays a role or if buoyancy
forcing is needed. It also raises the question whether
the bifurcation latitude is a robust feature that is closely
related to the gyre circulation, or if it is sensitive to local
winds and boundary flows.

In this work, we address these questions. We use
wind-driven layer models forced by different wind cli-

matologies and compare the annual cycle of the bifur-
cation latitude with the observational results from Qu
and Lukas (2003).

1.2 Models

The model studies by Qiu and Lukas (1996) using a
linear reduced gravity model were forced by the Florida
State University (FSU) wind stress (1961–1992) and
showed that the northern extreme occurred in October
and the southernmost position occurred in February.
That integration was close to being in phase with the
annual march of the latitude of zero wind stress curl,
but with much reduced amplitude. Applying a nonlin-
ear numerical model, Qiu and Lukas (1996) found a
somewhat larger amplitude than in the linear model
and a shift in phase so the southernmost latitude was
reached in March–April and the northernmost latitude
in October–November. Both their linear and non-linear
model results differ from the observations of Qu and
Lukas (2003) discussed in the previous section.

Qiu and Lukas (1996) also found that in the annual
mean, the bifurcation latitude was shifted about 0.5° to

the south of the annual mean of the zero wind stress curl latitude. From theory (McCreary and Lu 1994), it is seen that in case of a linear model with an active subsurface layer, the bifurcation latitude will in general not be located at the latitude of zero wind stress curl even in case of steady winds. They found that the bifurcation latitude for the transport field lies at the zero wind stress curl line only for an idealized wind stress field that is *independent* of latitude. It is therefore not clear from theory at which latitude the bifurcation should occur for flow in a realistic ocean model forced by seasonal winds.

1.3 Present research

In this paper, we demonstrate that the observed change in bifurcation latitude with season as well as the poleward shift with depth in the upper ocean can be reproduced in a wind-driven layer model. This implies that annual buoyancy forcing does not play an essential role for the bifurcation above the main thermocline. On decadal time scales or longer, buoyancy force is essential in maintaining the stratification. It is also of interest to determine if the bifurcation is sensitive to different wind climatologies, so a number of diverse wind products were used, and we also briefly explore if the shape of the coast line, local and remote forcing, or bottom topography plays an important role.

2 Numerical model

The ocean model is based on the multi-layer upper-ocean model (Jensen 1991, 1993), extended to include mixed layer physics and an option to include bottom topography (Jensen 1998, 2001). In the models used here, lateral stresses are proportional to the local deformation rate of the flow (Smagorinsky 1963) rather than constants as in previous versions. A Smagorinsky constant of 0.2 was used. Details about the model is given in Jensen (2001).

The model domain covers the global ocean north of 60° S to 60° N with a horizontal resolution of 1/4° and closed poleward boundaries. The configuration used for most experiments is a 4.5-layer reduced gravity model: It has four active layers with the average initial thickness of 80, 120, 250, and 600 m for layers 1 to 4, respectively. The deepest layer is infinitely deep and is at rest. The sigma-theta levels are chosen to be 23.6, 25.4, 26.5, 27.2, and 28.2 and are held constant in each isopycnal layer. In order to maintain a realistic layer thickness, upper limits and lower limits are imposed on each layer before mass is entrained or detrained

from adjacent layers. This is the hydromixing approach implemented in other layer models (e.g., Hurlburt et al. 1996). The layer thickness limits without entrainment are 50–120 m for layer 1, 80–200 m for layer 2, 120–250 m for layer 3, and 200–800 m for layer 4. Details of the method of constraining layer thickness as used in this model are given in Jensen (2001).

The reduced gravity model is the simplest configuration that extends the experiments by Qiu and Lukas (1996) to include a change of the bifurcation with depth. The advantage of this model is the relative low cost of integration, in spite of the high horizontal resolution needed for a good resolution of the bifurcation latitude. The relative simple model allows us to perform many experiments otherwise prohibitive due to high computational costs. A five-layer model configuration used to test potential impact of bottom topography is described in a subsequent section. Differences in the flows between the 4.5- and five-layer model configurations turn out to be relatively small in the upper fours layers in the area of interest, so we can use the purely baroclinic flows from the 4.5-layer model as reference.

3 Forcing for the control run and model spin-up

Climatological monthly mean wind stress from the European Centre for Medium Range Forecast (ECMWF) reanalysis (ERA-15) is used as forcing for a control run. The time period from 1979 to 1988 corresponding to the first Atmospheric Modeling Intercomparison Project was chosen. The wind stress is interpolated from the 2.5° spatial resolution to the ocean model grid using cubic splines and linear interpolation in time so it is updated each model time step.

A complete spin-up of the global ocean requires integration over several hundred years and is not feasible. By using a density stratification based on the annual average found in the vicinity of the bifurcation region computed from the World Ocean Atlas 94 (Levitus et al. 1994; Levitus and Boyer 1994), it is assumed that a thermal adjustment is not needed. Hence, there is no buoyancy forcing, so the model is purely wind-driven. The adjustment time for the model is set by propagation of Rossby waves across the basin (e.g., Gill 1982, pp. 507–512). The adjustment time for vertical mode n is

$$T_n = Lf^2/\beta c_n^2 \tag{1}$$

where L is the width of the basin, f the Coriolis parameter at a given latitude, β its variation with latitude, and c_n the internal wave speed of vertical mode

n. For the tropical and subtropical Pacific, the dominant vertical mode is the first baroclinic mode. The stratification above implies $c_1 = 3.6$ m/s, but using a more conservative estimate of $c_1 = 3$ m/s, allowing for layer adjustment to slow the waves, and a basin scale of $L = 15,000$ km gives a spin-up time of 6.2 years at 20° N as a minimum. Higher vertical modes have much longer adjustment times; for instance, the second internal mode wave speed is 1.62 m/s, requiring a minimum adjustment time of 21 years. However, the higher modes are also damped by friction which limits the adjustment time significantly for mode 3 and higher and prevents influence over large longitude ranges. Figure 2 shows the baroclinic sea surface height η computed for a 4.5-layer model (e.g., Jensen 2001, 2003):

$$\eta = \sum_{i=1}^{4} \frac{\rho_5 - \rho_i}{\rho_5}(H_i - H_{0i}) \qquad (2)$$

where ρ_i is the density, H_i the layer thickness, and H_{0i} the initial layer thickness at rest of layer i. This surface height includes contributions from all four baroclinic modes and provides a measure of the gyre circulation and its magnitude. As expected, the major circulation features in the tropical are present after 6 years. The subtropical gyres expand as the model continue to spin-up, although the differences are relative small between year 12 and year 20 in the tropics.

A concise discussion of basin adjustment times is given in McCreary et al. (2007). Using the same damping rate as in their work, the mode-2 damping time scale is very close to the mode-2 adjustment time for Rossby waves, i.e., 20 years.

We use the circulation after 20 years of spin-up as the control case. While this is too short to completely remove spin-up effects on the ocean gyres, it is sufficient to reproduce the basic flow features in the tropical and subtropical gyres. The model is eddy permitting with a
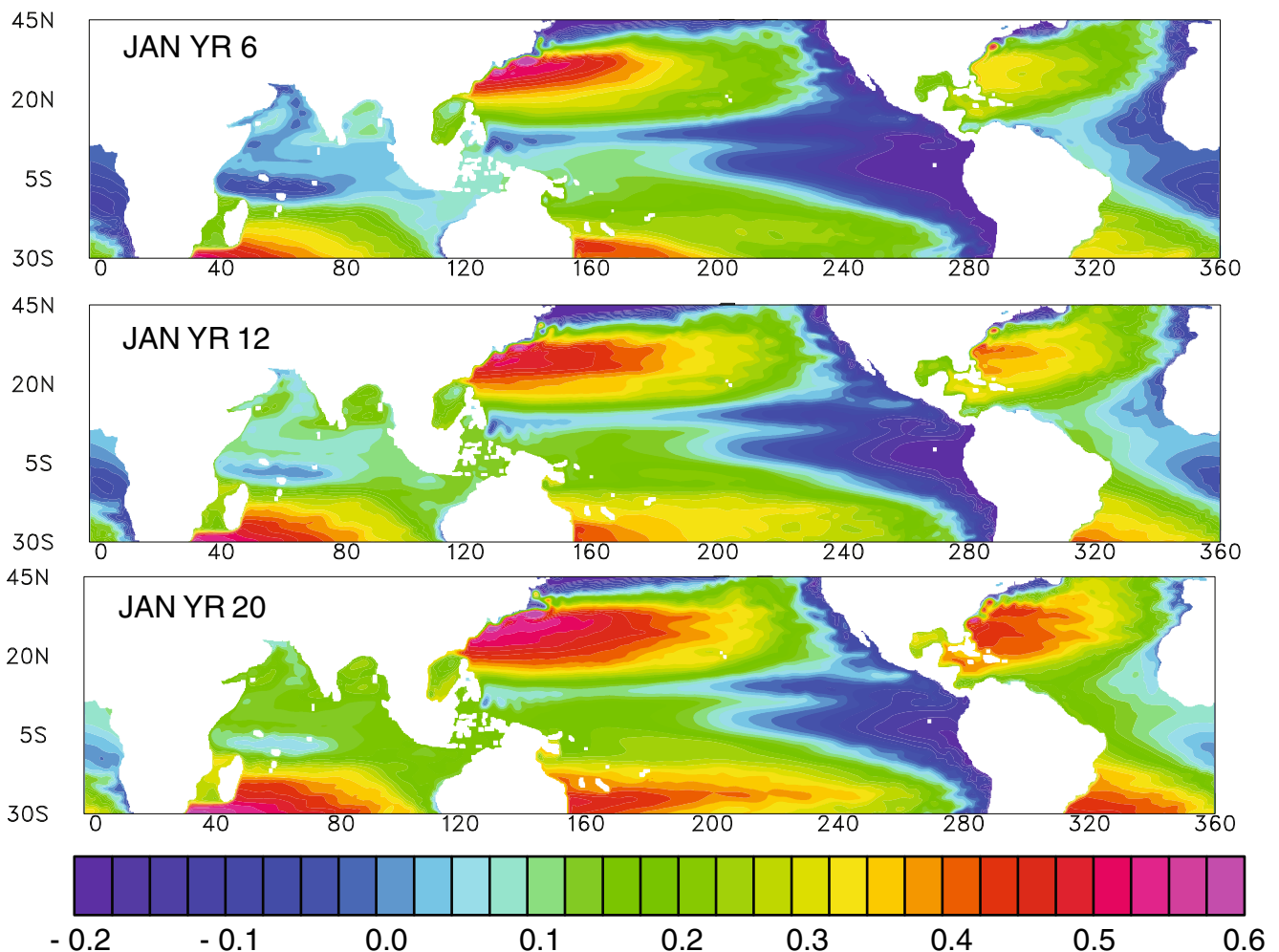
Fig. 2 Sea surface height displacement from initial condition using a 3-month average centered on January 6 on year 6 (*top*), year 12 (*center*), and year 20 (*bottom*) during the spin-up. Unit is meters

flow dependent low eddy viscosity, so a 90-day running average was made to the model fields before analysis.

4 Seasonal flow and transports

For the ECMWF, control run transports of the upper 850 m of three sections were computed. One section is from the Philippine coast to 140° E along 18° N. On the annual average, a northward Kuroshio transport of 13.5 Sv is found. The second section is across 140° E between 8° N and 18° N. The NEC transport in this section has an annual average of 36.1 Sv. The third section, from the coast along 8° N to 140° E, provides an estimate of the Mindanao Current transport of 14.1 Sv, a magnitude slightly above the model Kuroshio transport. Tozuka et al. (2002) also reported a near equal division of the NEC transport to the Kuroshio Current and Mindanao Current. Estimates from observational studies have found that the Mindanao transport exceeds the Kuroshio transport; for instance, Qu et al. (1998) reported it just over twice as large, while Kashino et al. (2009) found it larger by 29% and 60% during winters of 2006 and 2008, respectively. The model only includes the upper 850 m of the ocean in the bifurcation region, and there is a net subduction through the lowest layer of 8.5 Sv.

Figure 3 shows the monthly transport from the three sections. We find that the covariation between the NEC and the Mindanao Current is greater than between the

NEC and Kuroshio on a seasonal time scale. Simulations with an ocean general circulation model shows similar seasonal correlations (Kim et al. 2004). The currents in the layer model simulation agree well with the observed flow (Qu et al. 1998, 1999) and flow in general circulation models (Kim et al. 2004). Figure 4 shows the monthly mean currents when the bifurcation is in its northernmost position in January and in its southernmost position in July. These results increase our confidence in the simple wind-driven model for further analysis of the seasonal variation of the NEC bifurcation.

5 Bifurcation latitude changes with depth and season

For the model, we define the bifurcation point as a point of zero meridional velocity, calculated using 90-day running mean data for meridional velocities averaged from the coast to 126° E. Our results are only slightly dependent on this longitude, with less than 1/4° change in bifurcation latitudes if the longitude is changed by 1°. On the annual average, the change is much smaller. The bifurcation from our model is shown in Fig. 1 as filled in circles.

As in the observations, the model bifurcation latitude shifts poleward with depth. Kim et al. (2004) also found this to be the case in their OGCM results (see their Fig. 4). However, the change in bifurcation latitude with depth is the largest in the observations and the smallest in the OGCM.

Fig. 3 Transport of the NEC across 140° E between the latitudes 8° N and 18° N (*circles*) and transports between the coast of the Philippines and 140° E of the Mindanao Current across 8° N (*squares*) and the Kuroshio Current across 18° N (*triangles*)

1 m/s
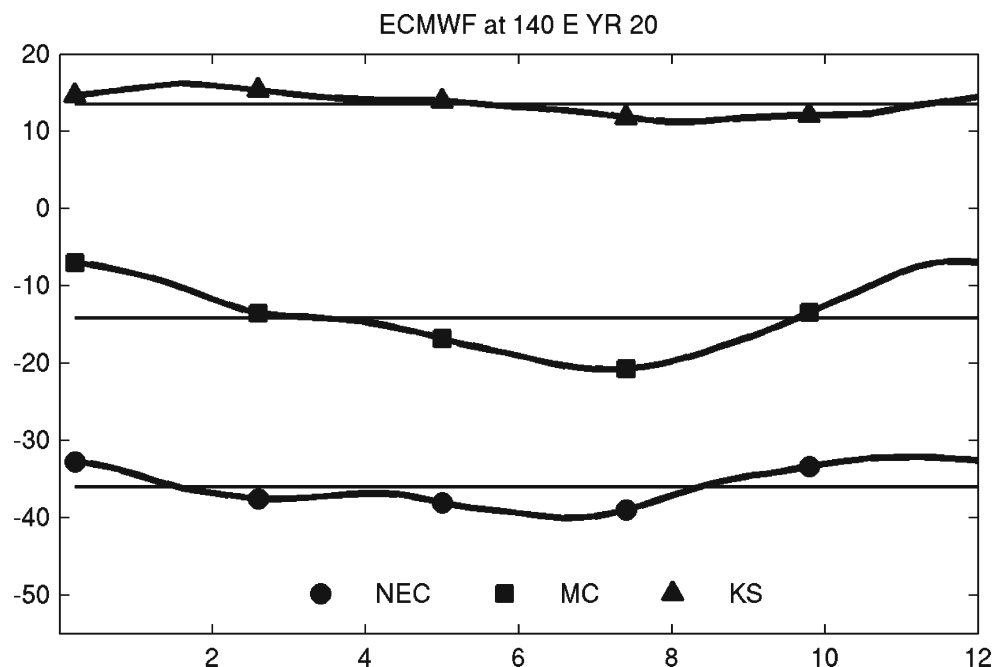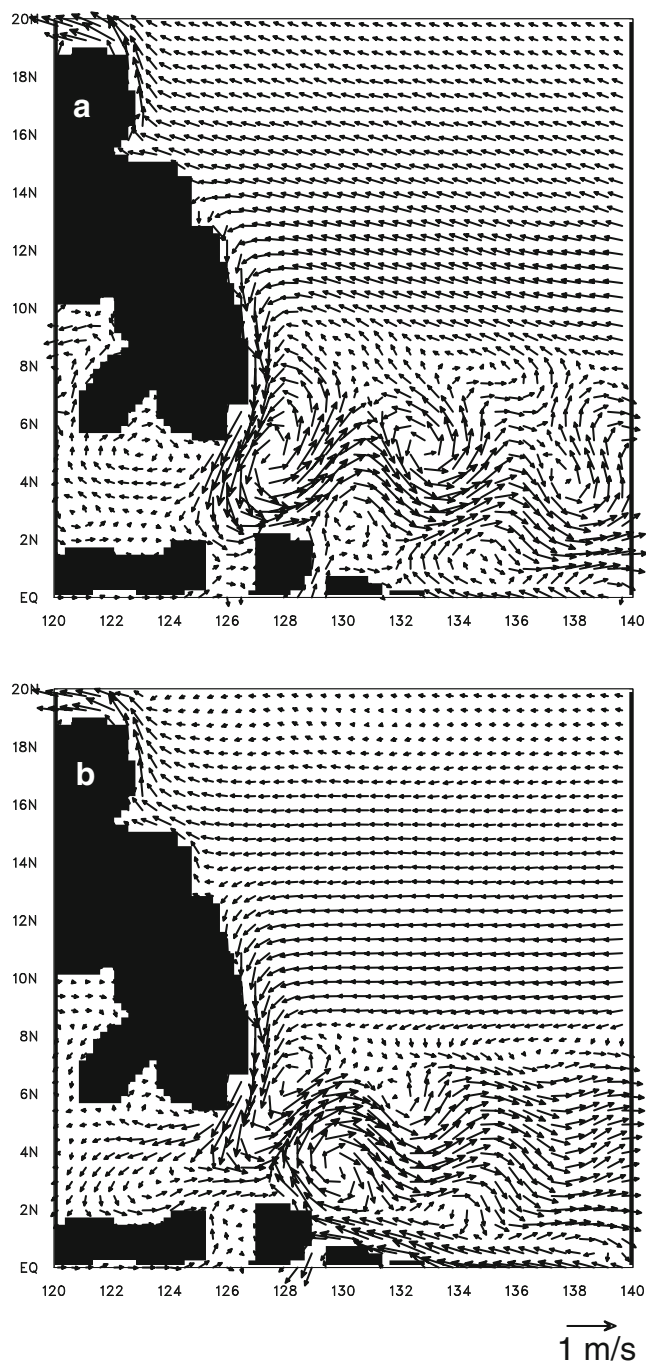
Fig. 4 Seasonal model currents in the upper layer on January 18 (**a**) and July 18 (**b**). A 90-day running average was applied. The length of each vector is proportional to the square root of the magnitude of the current. Unit is $(m/s)^{\frac{1}{2}}$

The seasonal cycle of the bifurcation is mainly controlled by a low dynamic height off the Philippines coast near 14° N during the northern winter which is associated with a southward flow anomaly along the coast. Figure 5 shows the sum of layer 1 and layer 2 thicknesses which is closely related to the dynamic height.

During the summer, this low is replaced by a positive dynamic height anomaly and associated poleward flow along the coast, showing a remarkable agreement with observations (Qu and Lukas 2003). This annual pressure anomaly is caused by a combination of remotely forced Rossby waves as well as a response to local winds (Qiu and Lukas 1996; Kim et al. 2004).

6 Wind stress climatologies

The 4.5-layer model was forced with other wind stress climatologies to investigate if the results above were sensitive to the wind stress product. As alternative forcings, we chose the Hellerman and Rosenstein (1983) wind stress (HR forcing), a monthly wind climatology using QuikSCAT winds from September 1999 to March 2002 (QS forcing), and wind stress from the FSU (1970–1999). They represent a range of wind stress products which have well-known advantages and problems. For instance, HR forcing is considered to be too strong in the tropics, but has been used in numerous model integrations. QuikSCAT scatterometer winds have high spatial resolution (0.5°), but cover too few years to be a representative climatology. It has been included here because of its high spatial resolution. The ECMWF ERA-15 wind stress used in the control is a relative coarse (2.5°) standard global reanalysis product, while the FSU wind stress is a highly quality controlled product based on ship observations. Both HR and FSU winds have a spatial resolution of 2.0°.

Figure 6 shows the Sverdrup transport streamfunction calculated for the four wind stress products. Note that the Hellerman–Rosenstein wind stress results in the largest transport, followed in strength by the ECMWF and the FSU wind stress climatologies. The QuikSCAT wind stress is significantly weaker than the other wind stress products south of 12° N. The annual average line of zero Sverdrup transport is at 14° N for the QuikSCAT wind stress while it is about 1° further poleward for the other wind stress products. The QuikSCAT wind stress used here is dominated by strong La Niña conditions, which tends to shift the bifurcation equatorward (Kim et al. 2004).

7 Sensitivity to wind climatology

Figure 7 shows the bifurcation latitude for the upper three model layers, using four different wind stress climatologies: the classic and commonly used Hellerman and Rosenstein (1983) in Fig. 7a, the ECMWF forcing used as our forcing for control runs in Fig. 7b, the

Fig. 5 Seasonal anomaly of the sum of layer 1 and layer 2 thickness (meters) and anomaly transports (vectors) in those two layers for DJF (**a**) and JJA (**b**). The vectors has been re-scaled by taking the square root of the magnitude so the unit is $(m^2/s)^{1/2}$

ECMWF 1977-1988

Hellerman-Rosenstein

**FSU 1977-1999**

Quick Scat 1999-2001
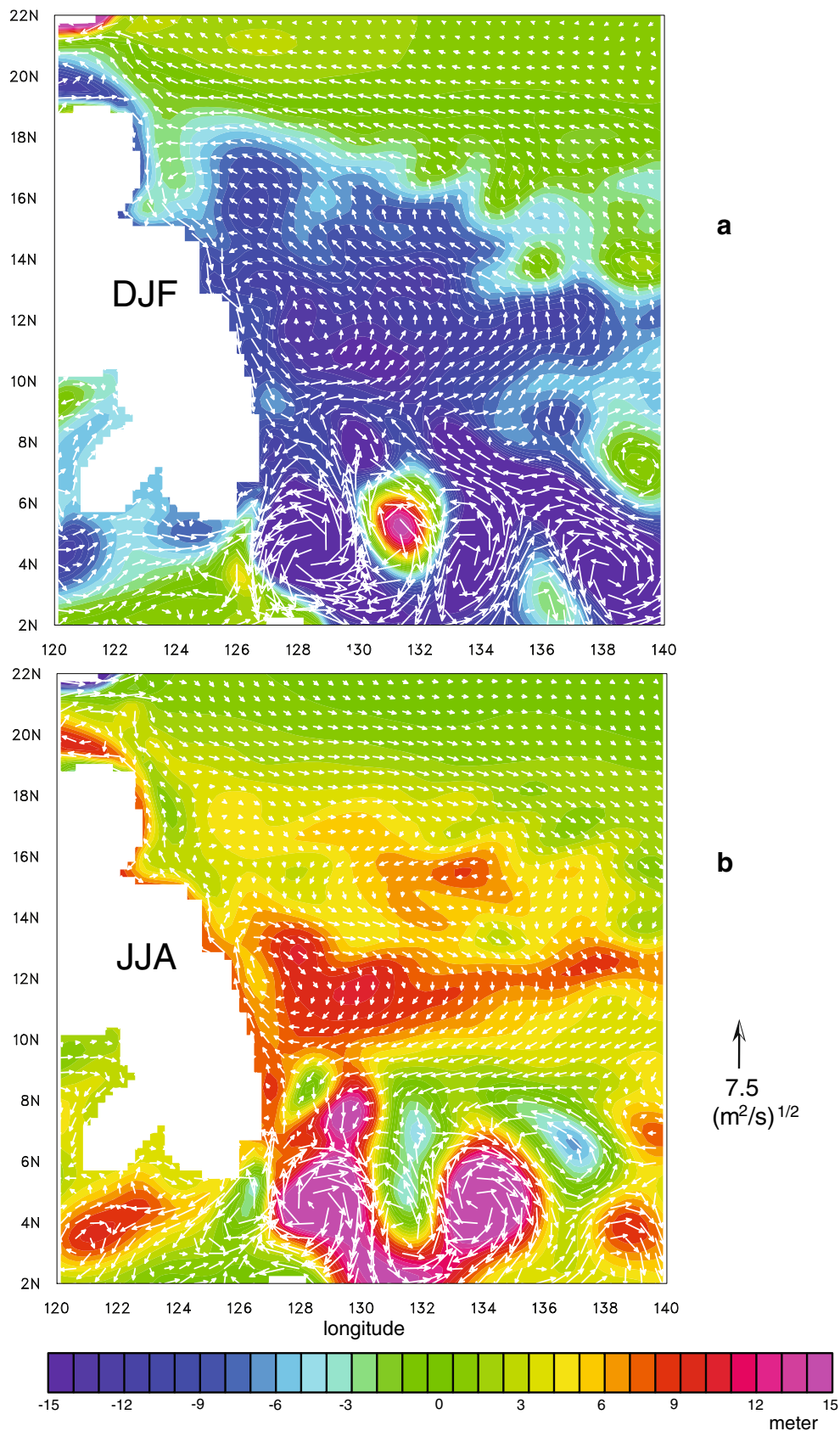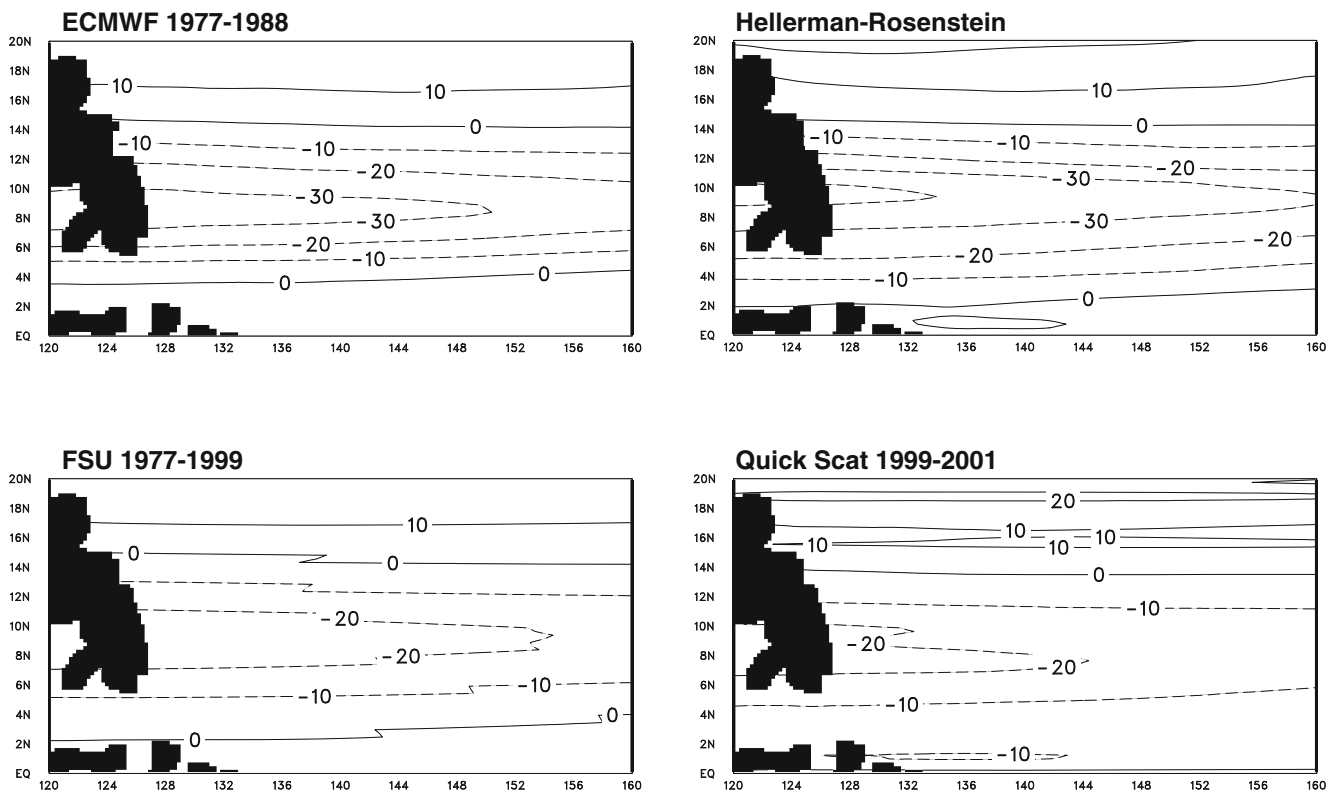
Fig. 6 Sverdrup transport for four different wind stress products used in the simulations. Unit is Sverdrup

FSU 1979–1999 forcing in Fig. 7c, and the QuikSCAT forcing in Fig. 7d. The panels are arranged based on the extreme southward latitude of the surface layer bifurcation for a given climatology. The bifurcation latitude for each layer is determined by taking the average meridional transport from the coast to 126° E and searching for a sign change between 10° N and 19° N.

In layer 4, which represents flow at about 850 m, the eddy field dominates the flow, and a unique bifurcation is most often not identifiable during the summer, as also noted by Qu and Lukas (2003). During winter, bifurcations in layer 4, north of the layer 3 bifurcations, were found in most years, but variability from year to year does not provide confidence in their significance.

Fig. 7 Bifurcation latitude by month for layers 1 to 3 when forced by different climatologies. Layer 1: *full*, layer 2: *dashed*, layer 3: *dash-dot*. From *left to right*: Hellerman–Rosenstein (**a**), ECMWF (**b**), FSU (**c**), and QuikSCAT (**d**)
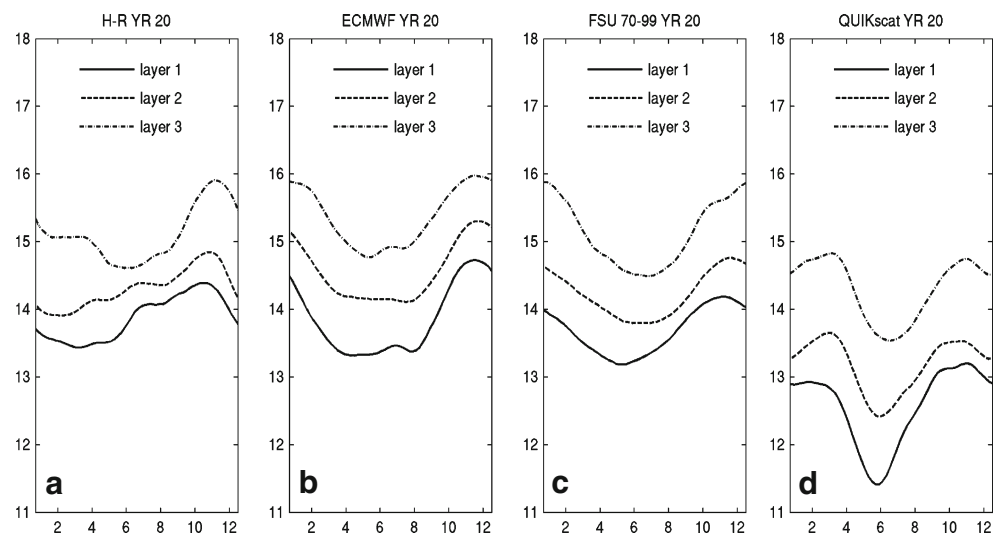
The following discussion will compare the bifurcation for the other three cases to the bifurcation in the control case forced by ECMWF winds (Fig. 7b). For the surface layer, the southernmost latitude is found from April through August and the northernmost position in December. The bifurcation of the subsurface layers is closest to the equator in June to August and at its most poleward position in November and December. This seasonal cycle corroborates the analysis of Qu and Lukas (2003). Agreement between their observations and our model varies with depth: It is at the observed latitude in the upper layer, which is centered at a depth around 50 m, and directly affected by the wind stress. In the second model layer, which is mainly geostrophically driven, the bifurcation in the model is about 1° closer to the equator than observed. At intermediate depth, about 450 m, the observed bifurcation is 2° further poleward in the summer and 3° further poleward in the winter. The change with depth of the bifurcation latitude is 1.5° in this model run, but is a factor of two larger in the observations (Fig. 1).

Figure 7a shows that the amplitude of the seasonal cycle is much reduced using the HR forcing, although the phase in the deepest layer is similar with that for the ECMWF winds. The equatorward displacement during the summer is absent for the upper layers. The southernmost bifurcation takes place in March for the uppermost layer and in February for layer 2. A poleward shift in latitude with depth is reproduced, but is less than in the control case. In contrast, the QS forcing produces a model response with larger change of the bifurcation latitude with depth, about 3.5°, and a bifurcation 1.5° closer to the equator. The seasonal cycle has a larger amplitude with its southernmost position in June and northernmost positions in March and in November. (Fig. 7d).

The response to the FSU forcing (Fig. 7c) is in between the ECMWF and QuikSCAT responses in terms of the range of bifurcation change with depth. However, the amplitude of the annual cycle of the bifurcation latitude is about the same for the four different cases, about 1.5°, while the observations by Qu and Lukas (2003) show a range of 2.5°.

In Fig. 7, the results are ordered from left to right using wind stress climatologies with increasing magnitude of the Sverdrup transport , i.e., Fig. 6. Note that the stronger wind stress curl, i.e., HR and ECMWF forcing, result in a bifurcation further to the north for layers 1 and 2 and with less depth dependence than the weaker wind stress climatologies, e.g., FSU and QuikSCAT.

A 6-year simulation with the QuikSCAT wind stress reduced globally by a factor of 2 (not shown), moved the bifurcation latitude further southward by about 1°

for layers 1 and 2 with no change in phase. In layer 3, the bifurcation occurred less than 0.5° further south, while a poleward shift of about 1° was found in layer 4. While the bifurcation of the depth-integrated flow moved equatorward by 0.5° after reducing the strength of the wind stress by a factor of 2, the poleward shift in bifurcation with depth was increased as the strength of the forcing was decreased. We find that this tendency of increased depth dependency and equator shift in bifurcation with weaker wind stress to be general for our reduced gravity model results.

8 Local and remote forcing

The Southeast Asian monsoon has a dominant wind component from the south during May through September, while the meridional wind component is from the north in the remainder of the year. This reversal extends eastward to about 140° E.

The influence of remote forcing by annual Rossby waves is clearly seen from Fig. 8 that displays monthly maps of the correlation between sea surface height (SSH) with SSH_{local}, defined as the area averaged SSH over a small region bounded by 124° E to 126° E and 14.5° N to 15.5° N near the bifurcation latitude. A large positive correlation approaches from the northeast of the bifurcation and is at 20° N at lag minus 2 months with a propagation consistent with a first baroclinic Rossby wave signal. Positive lags show coherent SSH anomalies along the coast after the impact of the Rossby wave. It is clear that remote forcing plays an essential role for the bifurcation.

In order to determine the relative importance of local and remote forcing, we define a *local area* bordered by longitudes 120° E to 140° E and latitudes 5° N to 20° N. Around the local area, we define a 10° wide *buffer zone*, while the remaining model domain is defined as the *remote area*. We made two integrations: a *local forcing* experiment, where ECMWF monthly winds were used in the *local area*, and annual averaged wind stress in the *remote area*. In the buffer zone, a linear interpolation between monthly wind and annual averaged wind was used. In the *remote forcing* experiment, annual averaged forcing was used in the *local area* and monthly forcing in the *remote area* with linear interpolation in the *buffer zone*.

When the wind forcing is allowed only to vary with time within the *local area*, the winter low pressure anomaly in the upper ocean is weakened compared to the control case (not shown), and the response to the annual march of the southeast asian monsoon is much
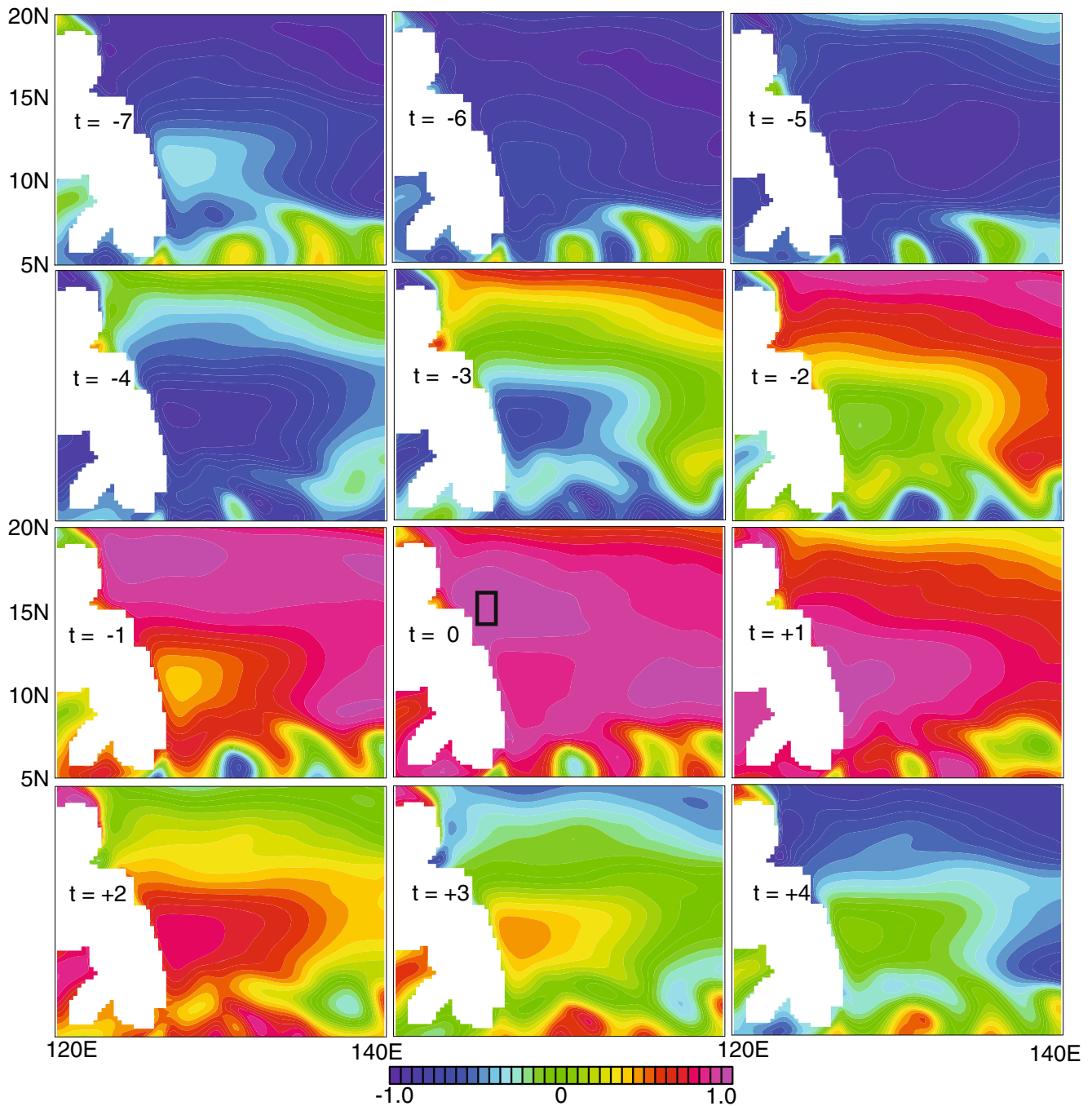
Fig. 8 Correlation maps of monthly SSH with the area averaged SSH$_{local}$, computed over the bifurcation region (124° E–126° E, 14.5° N–15.5° N) shown by a *black rectangle* in the panel with zero lag. Monthly lags are shown from negative 7 (*upper left*) where SSH$_{local}$ leads, to a positive lag of 4 months where SSH$_{local}$ lags (*lower right*). The solution is from year 20 and was forced by the ECMWF wind stress

faster (Fig. 9a) than in the control case (Fig. 7b), i.e., there is a phase shift such that the extreme bifurcation latitudes occur about a month earlier. For instance, as the positive wind stress curl weakens in the late winter just northeast and east of the bifurcation region and the line of zero wind stress curl move southward, the bifur- cation latitude rapidly moves southward in response. A fast return northward takes place in November when the positive wind stress curl returns. In contrast, when only the wind east of 140° E has an annual cycle, the bifurcation response is delayed by 1 to 2 months in the upper ocean (Fig. 9b). When monthly forcing is

Fig. 9 Bifurcation latitude by month for layers 1 to 3 when forced by ECMWF wind stress. Layer 1: *full*, layer 2: *dashed*, layer 3: *dash-dot*. From *left to right*: Monthly local winds and annually averaged remote winds (**a**), monthly remote winds and annually averaged local winds (**b**), as control run, but with a straight Philippine coast (**c**), and as 4.5 layer model control run, but with bottom topography included (**d**)
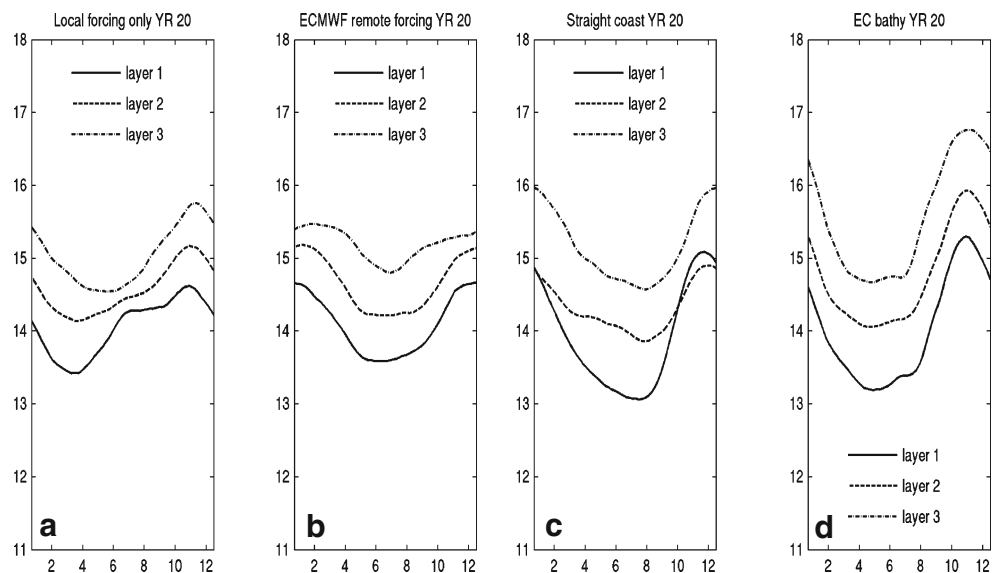
applied to the entire ocean, the time span where the bifurcation latitude is near its extremes is significantly longer (Fig. 7b). The Mindanao Dome is southeast of the bifurcation and is part of the bifurcation problem. Tozuka et al. (2002) demonstrated how local positive wind stress curl produced upwelling during spring was important for generating the Mindanao Dome, and its damping later in the year was caused by downwelling generated by remote negative wind stress curl. Our results are consistent with their findings.

Fig. 10 Bottom topography used in the five-layer model is shown near the Philippine coast. The depth of the ocean varies from 1,500 to 5,500 m in the model. Contour interval is 150 m
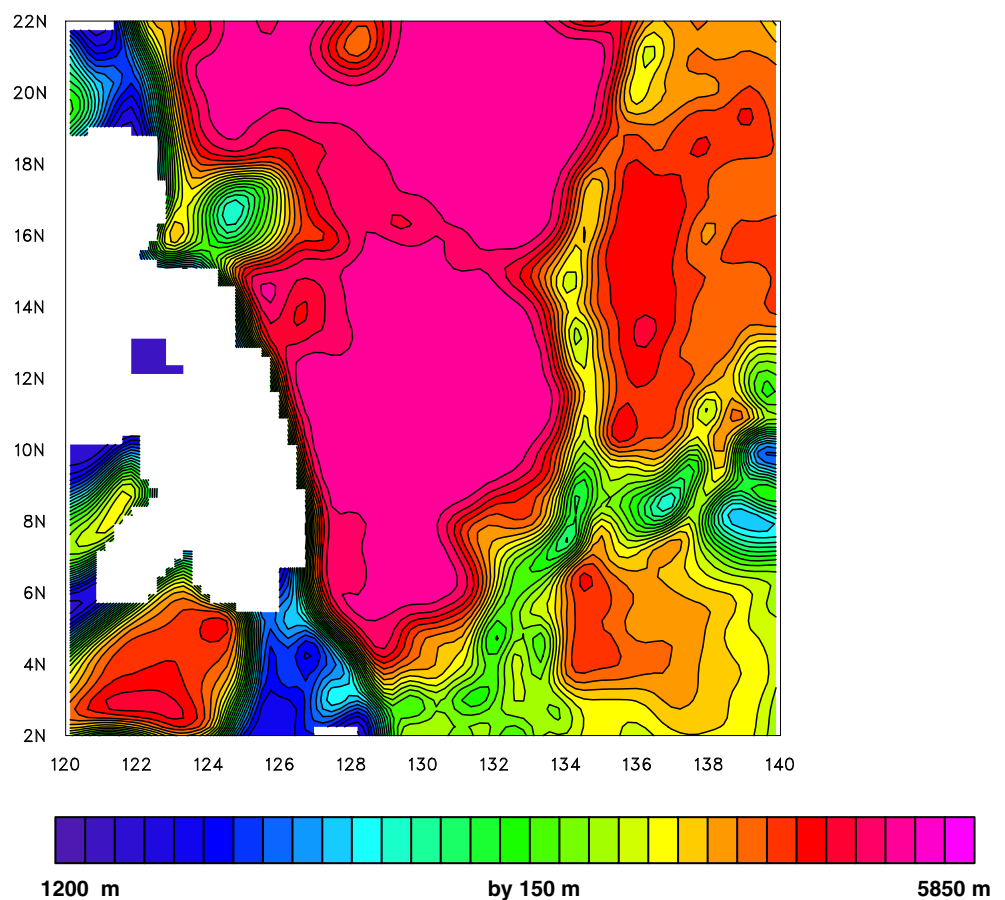
9 Sensitivity to shape of coast and bottom topography

In this section, the sensitivity to the shape of the coast lines and to bottom topography is briefly addressed. The model runs with modified coastlines and bottom topography were done with the same ECMWF wind forcing as in the control run. The model Philippine coast line varies from about 127° E at 6° N to 122.5° E at 18° N. To determine if the shape of the coastline has an influence on the bifurcation, a model geometry with a straight coastline situated at 125° E was used in the model. The effect of reshaping the coast is relatively small for the poleward displacement with depth as seen by comparing the bifurcation when a realistic coastline is used (Fig. 7b) with the case when a straight coastline is used (Fig. 9c). However, the bifurcation latitude minimum is delayed until August and is 0.25° further to the south, resulting in a more pronounced minimum latitude. During the fall, the bifurcation latitudes of the layer 1 and layer 2 flows are essentially at the same latitude. Overall, the influence of the shape of the coastline is small.

To determine the effect of bottom topography, a five-layer version of the model was used. This model

Fig. 11 Difference between the annual average flow in the five-layer model and the 4.5-layer model when forced with ECMWF winds in layer 1 (*top*) and in layer 4 (*bottom*)
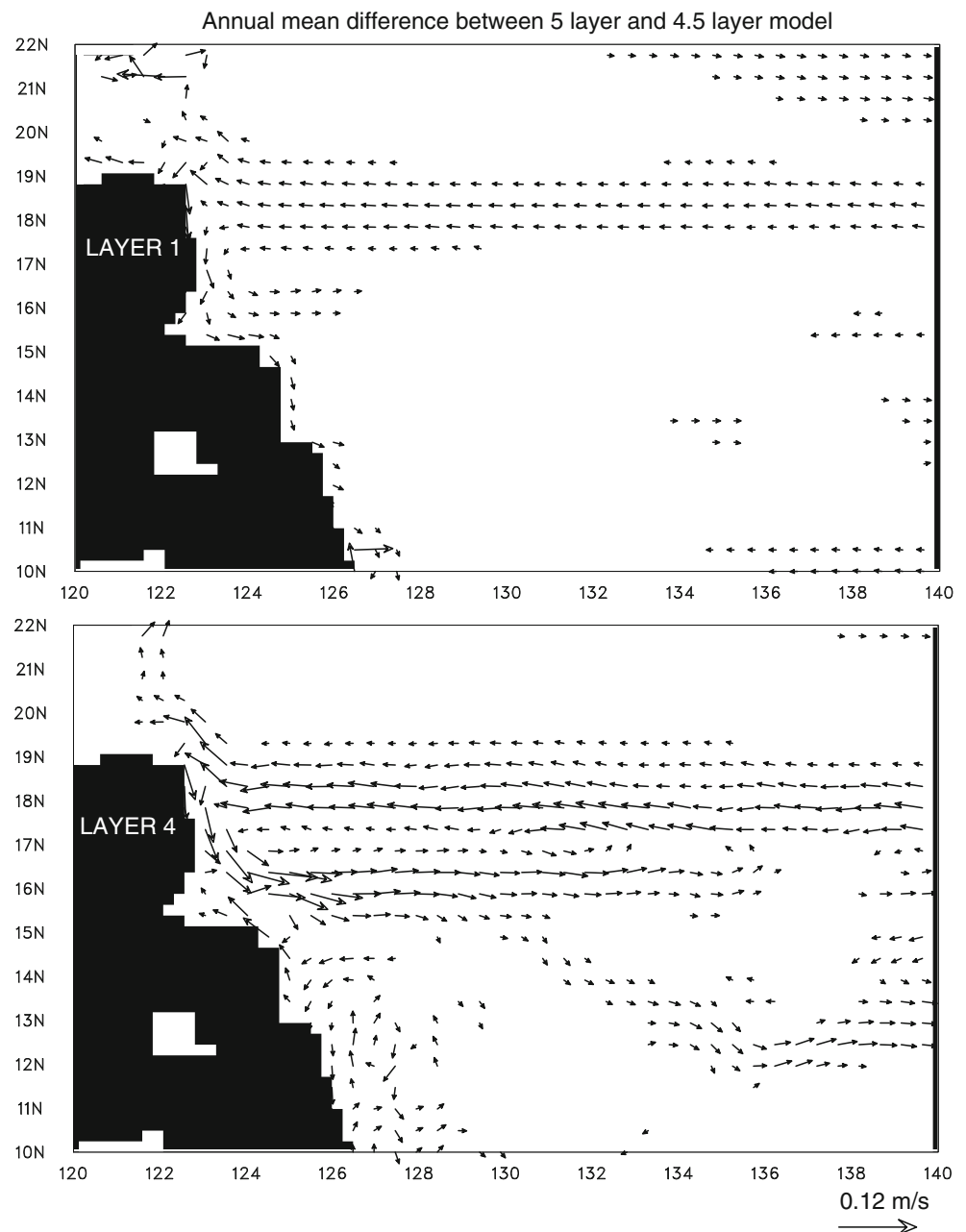
is identical to the 4.5-layer model, except that a finite depth with realistic bottom topography is used below 1,200 m in the entire model domain. The local bottom topography is shown in Fig. 10. The numerical method used is the gravity wave retardation method (Jensen 1996) with a speed up factor of 8 for the barotropic gravity waves. This method has been shown to give realistic flow over deep topography (Jensen 2001, 2003).

Introduction of bottom topography has three effects: The finite depth slows down the baroclinic wave speeds compared to the reduced gravity model: Near 155° E, the first vertical mode baroclinic planetary wave speed is 0.59 m/s for the 4.5-layer model and 0.52 m/s for the five-layer model. Near the coast, at 130° E, the phase speeds have increased to 0.73 and 0.69 m/s, respectively. Secondly, it adds a barotropic flow that in the absence of stratification would follow f/D contours, where D is the ocean depth. Stratification limits the importance of local topography, but can still affect the upper layers through the joint effect of baroclinicity

and relief (JEBAR). Cane et al. (1998) have given a very useful interpretation that JEBAR has an effect on the barotropic flow when there is a near-bottom geostrophic flow up or down the topographic slopes (see their Eq. 2), an explanation that is particularly applicable to layer models. Thirdly, interfacial friction between the deepest layer and the upper layers, layer 4 in our case, is affecting the strength of the coupling between the deep and the upper ocean.

For the upper three layers, the influence of topography is small for the flow away from the boundary, suggesting at first that bottom topography effects are unimportant. However, when the bifurcation is computed, a shift in phase is seen (Fig. 9d). Figure 11 shows differences between the five-layer model and the 4.5-layer model simulation for the annual averaged flow for year 20 in layer 1 and in layer 4. The differences are mainly due to the additional barotropic component of the flow in the finite depth model, and consequently, the differences between the two model solutions in

Fig. 12 Annual average flow in the abyssal layer during year 20 from the model simulation with bottom topography. The contours show the 2,000- and 3,000-m isobath (*dashed lines*) and the 4,000-m isobath (*full line*)
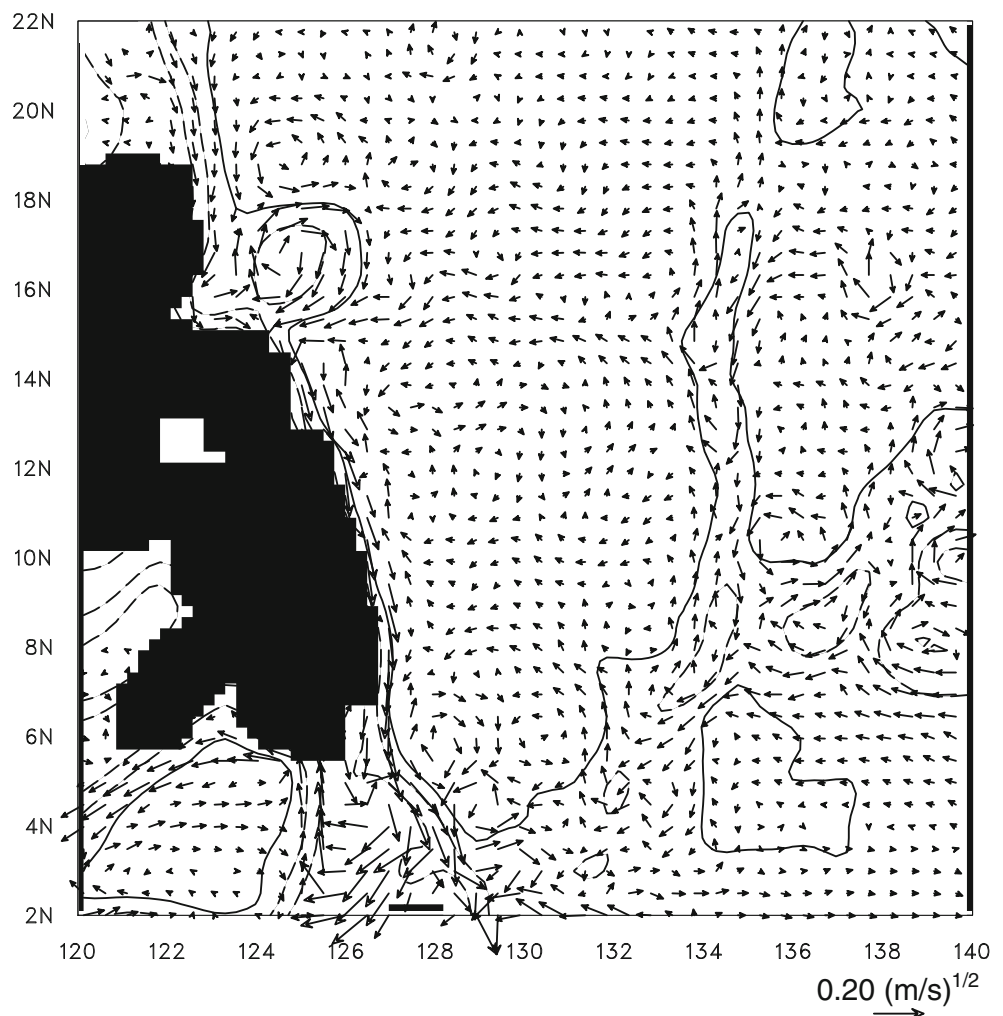
layer 2 and layer 3 (not shown) are very close to those found in layer 1. There is an enhanced westward flow in the northern part of the NEC and a decrease in current velocity in its southern part. This flow anomaly is more enhanced during the winter and leads to a northward shift in the bifurcation latitude during the fall and winter (Fig. 9d) compared to the control case (Fig. 7b). Another difference between the finite depth run and reduced layer model run is in the phase speed of westward propagating Rossby waves. The differences are fairly small, and with the slower propagation in the case with topography, a lag in phase of the bifurcation compared to the 4.5-layer case would be expected. Rather, the extrema occur about a month earlier, suggesting that the propagation speed differences are not important. Finally, the topography close to the Philippine coast features a seamount centered at 125° E, 16.5° N, which has an anti-cyclonic circulation throughout the year. Figure 12 shows this anti-cyclonic circulation and the abyssal (layer 5) annual mean flow in the domain of interest. The seamount does not affect the bifurcation significantly, and as indicated by the flow in layer 4 (Fig. 11, bottom panel), there is no indication the seamount has any influence on the upper layers. The abyssal flow is southward along the Philippine coast and forms an anticlockwise circulation with northward flow along the western side of the Palau Ridge and westward flow beneath the NEC. The flow is primarily along the isobaths in the annual mean, but up- and downslope flows occur throughout the year suggesting some influence of JEBAR. However, to a large extent, the deep flow is decoupled from the flow in the upper layers.

10 Discussion

Earlier modeling work using wind-driven models (e.g., Qiu and Lukas 1996) did not explore the change of the bifurcation with depth and found a seasonal change that does not agree with recent analysis of observations (Qu and Lukas 2003). As demonstrated in this paper, a global model with additional layers–and therefore additional baroclinic modes, gives results in good agreement with observations. Do the additional baroclinic modes make the difference? Experiments with a 1.5-layer version of the model reduced the annual amplitude of the bifurcation latitude, but did not change its phase. In order to further explore this, Miyama et al. (2003) used a 1.5-layer model with the same domain as Qiu and Lukas (1996), i.e., Pacific Ocean only and identical forcing (FSU 1961–1992; Fig. 13). They found that the bifurcation latitude was sensitive to the model's domain size. With a southern boundary at 15° S, a run was done with the northern boundary at 60° N, and was compared with a run with the northern boundary at 40° N the

Fig. 13 Seasonal variations of the bifurcation latitude in a linear 1.5-layer model with the northern model boundary at 60° N (*full line*), with northern boundary at 40° N (*dashed line*) as in Qiu and Lukas (1996) and with the northern boundary at 40° N and strong damping applied (*dotted line*). From Miyama et al. (2003)
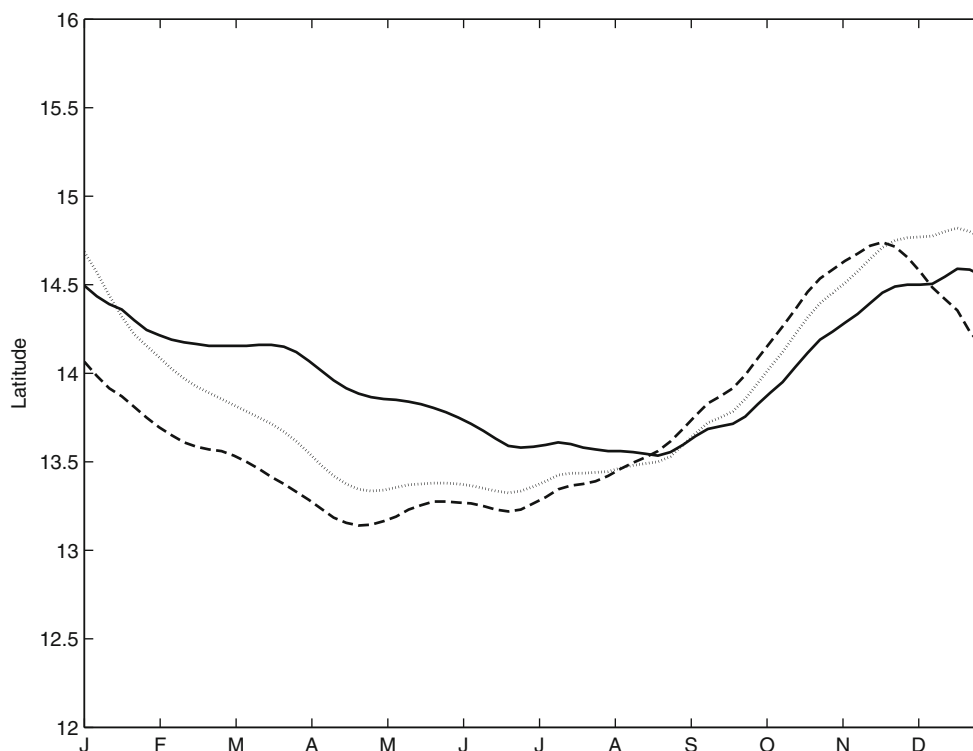
latitude as was used by Qiu and Lukas (1996). The second run shows a shift of the most equatorward bifurcation latitude from late summer to early spring. The earlier response was due to a spurious coastal Kelvin wave that propagated the effects of remote winds westward at a faster rate than possible by Rossby waves (Miyama et al. 2003). They also made an experiment with strong horizontal eddy viscosity along the boundaries as used by Qiu and Lukas (1996), but that did not improve the result very much (Fig. 11). We therefore suspect the result by Qiu and Lukas (1996) was influenced by their artificial boundaries.

The 4.5-layer model results agree quite well with the observed seasonal cycle of the bifurcation latitude and its variation with depth. As in the analysis by Qu and Lukas (2003), a depth of no motion is implicitly given in the 4.5-layer model.

Experiments where only annual mean wind forcing was used east of 140° E provided a scenario where only local seasons had an influence. This resulted in shorter duration of the time where the bifurcation latitude was at its extremes. The southernmost and northernmost bifurcation was found earlier than observed, implicating that remote forcing is needed to get the correct phase.

An experiment with straight coastline demonstrated some impact on the bifurcation, but indicates that the local boundary condition is of less importance than the forcing. A five-layer model simulation including bottom topography produced a northward shift in bifurcation during fall and winter due to inclusion of the barotropic mode. The seasonal phase of the bifurcation was leading that of the 4.5-layer model by about a month, a result that is in less agreement with observations than the 4.5-layer model results. However, inclusion of finite depth and bottom topography did not substantially alter our results for the upper layer flow.

All model simulations were run without seasonal buoyancy forcing, but only a vertical hydromixing that ensures the model stratification does not change much from the initial conditions. This suggests that the bifurcation latitude is determined by the wind stress and transferred to the deeper ocean via baroclinic waves. Different wind climatologies produce qualitatively similar results, but also show one important difference: Stronger wind stress results in a bifurcation further poleward.

Finally, it should be noted that inter-annual variability of the bifurcation latitude associated with ENSO has been found in modeling studies and has recently been observed. Modeling studies by Kim et al. (2004) found a northward shift in the position of the bifurcation during El Niño and a southward shift during La Niña. Observations by Kashino et al. (2009) did not find a significant difference in the bifurcation latitude during the 2006–2007 El Niño and the 2007–2008 La Niña, but did find increased North Equatorial Current and Mindanao Current transports.

Overall, the seasonal cycle of the bifurcation latitude is fairly robust, and the annual average bifurcation latitude differs less than 0.5° between the runs forced with different climatological wind stress products. An exception is the run forced with QuikSCAT winds. However, this wind forcing was chosen as a short non-representative climatology, suggesting that the bifurcation is subject to inter-annual variability.

References

Cane MA, Kamenkovich VM, Krupitsky A (1998) On the utility and disutility of JEBAR. J Phys Oceanogr 28:519–526

Gill AE (1982) Atmosphere–ocean dynamics. Academic, San Diego, 662 pp

Hellerman S, Rosenstein M (1983) Normal monthly wind stress over the world ocean with error estimates. J Phys Oceanogr 13:1093–1104

Hurlburt HE, Wallcraft AJ, Schmitz Jr WJ, Hogan PJ, Metzger EJ (1996) Dynamics of the Kuroshio/Oyashio current system using eddy-resolving models of the North Pacific Ocean. J Geophys Oceans 101:941–976

Jensen TG (1991) Modeling the seasonal undercurrents in the Somali current system. J Geophys Res 96:22151–22167

Jensen TG (1993) Equatorial variability and resonance in a wind-driven Indian Ocean model. J Geophys Res 98:22533–22552

Jensen TG (1996) Artificial retardation of barotropic waves in layered ocean models. Mon Weather Rev 124:1272–1283

Jensen TG (1998) Description of a Thermodynamic Ocean Modelling System (TOMS). Atmospheric Science Paper, No 670: 50 pp, Colorado State Univ., Fort Collins, Colorado

Jensen TG (2001) Application of the GWR method to the tropical Indian ocean. Mon Weather Rev 129:470–485

Jensen TG (2003) Barotropic mode errors in an Indian Ocean model associated with the GWR method. Glob Planet Change 37:1–18

Kashino Y, Espana N, Syamsudin F, Richards KJ, Jensen T, Dutrieux P, Ishida A (2009) Observations of the North Equatorial Current, Mindanao current, and Kuroshio current system during the 2006/07 El Niño and 2007/08 La Niña. J Oceanogr 65:325–333

Kim YY, Qu T, Jensen T, Miyama T, Mitsudera H, Kang H-W, Ishida A (2004) Seasonal and interannual variations of the North Equatorial Current bifurcation in a high-resolution OGCM. J Geophys Res 109:C03040. doi:10.1029/2003JC002013

Levitus S (1982) Climatological Atlas of the World Ocean. NOAA Professional Paper No. 13. U.S. Government Printing Office, Washington D.C., 163 pp

Levitus S, Boyer T (1994) World Ocean Atlas 1994, vol 4: temperature. NOAA Atlas NESDIS 4. U.S. Gov. Printing Office, Washington, D.C., 117 pp

Levitus S, Burgett R, Boyer T (1994) World Ocean Atlas 1994, vol 3: Salinity. NOAA Atlas NESDIS 3. U.S. Gov. Printing Office, Washington, D.C., 99 pp

McCreary JP, Lu P (1994) Interaction between the subtropical and equatorial ocean circulation: the subtropical cell. J Phys Oceanogr 24:466–497

McCreary JP, Miyama T, Furue R, Jensen T, Kang H-W, Bang B, Qu T (2007) Interactions between the Indonesian throughflow and circulations in the Indian and Pacific oceans. Prog Oceanogr 75:70–114

Miyama T, McCreary JP, Kim YY, Jensen TG, Qu T, Ishida A (2003) What controls the seasonal variation of the Pacific North Equatorial Current bifurcation latitude? Abstract. Spring meeting of the Oceanographic Society of Japan Tokyo, Japan

Nitani H (1972) Beginning of the Kuroshio. In: Stommel H, Yoshida K (eds) Kuroshio: physical aspects. University of Tokyo Press, Tokyo, pp 129–163

Qiu B, Lukas R (1996) Seasonal and interannual variability of the North Equatorial Current, the Mindanao current, and the Kuroshio along the Pacific western boundary. J Geophys Res 101:12315–12330

Qu T, Lukas R (2003) On the bifurcation of the North Equatorial Current in the Pacific. J Phys Oceanogr 33:5–18

Qu T, Mitsudera H, Yamagata T (1998) On the western boundary currents in the Philippine sea. J Geophys Res 103:7537–7548

Qu T, Mitsudera H, Yamagata, T (1999) A climatology of the circulation and watermass distribution near the Philippine coast. J Phys Oceanogr 29:1488–1505

Smagorinsky J (1963) General circulation experiments with the primitive equations. I. The basic experiment. Mon Weather Rev 91:99–164

Toole JM, Millard RC, Wang Z, Pu S (1990) Observations of the Pacific North Equatorial Current bifurcations at the Philippine coast. J Phys Oceanogr 20:307–318

Tozuka T, Kagimoto T, Masumoto Y, Yamagata T (2002) Simulated multiscale variations in the western tropical Pacific: the Mindanao dome revisited. J Phys Oceanogr 32:1338–1359